Silicon Nanotube Array/Gold Electrode for Direct Electrochemistry of Cytochrome c

ARTICLE *in* THE JOURNAL OF PHYSICAL CHEMISTRY B · MARCH 2007

Impact Factor: 3.3 · DOI: 10.1021/jp0657944 · Source: PubMed

Silicon Nanotube Array/Gold Electrode for Direct Electrochemistry of Cytochrome *c*

Cheng Mu, Qiang Zhao, Dongsheng Xu,* Qiankun Zhuang, and Yuanhua Shao*

Beijing National Laboratory for Molecular Sciences, State Key Laboratory for Structural Chemistry of Unstable and Stable Species, College of Chemistry and Molecular Engineering, Peking University, Beijing 100871, China

Received: September 6, 2006; In Final Form: November 21, 2006

The highly ordered Si nanotube (SiNT) arrays have been fabricated and demonstrated to be an attractive matrix to accommodate macromolecules, such as proteins, and exhibit facile direct electrochemistry of cytochrome *c* without any pretreatment. A pair of well-defined redox waves can be observed in the aqueous solution containing cytochrome *c* on this SiNT electrode using cyclic voltammetry. The peak separation (ΔE_p) between the anodic and the cathodic peaks is 63 mV at the sweep rate of 10 mV/s, and the peak current is proportional to the square root of the sweep rates, which indicates that the redox process is a quasi-reversible process. The experimental results show that the good biocompatibility and nanoscale hollow structure of the SiNT arrays can be applicable to preparing Si-based biosensors and protein characterizations.

Introduction

The achievement of mediator-free communication between the prosthetic groups of redox proteins and an electrode surface is of great interest both in fundamental investigations of the mechanism of biological redox reactions and in development of novel biosensors and bioelectrocatalytical devices.[1−4] The kinetics of the redox reactions of proteins on an electrode are known to be strongly dependent upon a combination of interfacial electrostatic and chemical interactions, which are derived from the protein structure and the nature of the electrode surface. In general, direct electrochemistry of redox proteins on bare or "naked" solid electrodes has been proven to be very difficult due to the deeply buried redox center and instability of the biological matrix upon interaction with the electrode surface.

Chemically modified electrodes with appropriate coatings can provide a protective environment for proteins and improve the stability of the entrapped proteins, thus facilitating direct electron transfer (ET).[5−9] For proteins confined within small cavities or in crowded environments, spatial confinement that occurs on the surface may raise barriers of all dynamic processes in the protein, eliminate some extended configurations, and shift the equilibrium from the unfolded state toward the native state. For this purpose, many nanomaterials including Au nanoparticles, nanopore SnO_2, TiO_2, and Nb_2O_5 films, and carbon nanotubes have been applied as candidates for the immobilization of redox proteins and also as electrodes for direct electrochemistry of such proteins.[6,9−14] Recently, various ionic liquids have been combined with carbon nanotubes to form conductive gel, which can be employed to investigate the electrochemical behaviors of cytochrome *c*.[15] In addition, because of the larger surface area and the smaller size, nanomaterials may decrease the diffuse distance for the substrate to access the immobilized proteins, thus promoting the kinetics of the redox proteins on an electrode surface.

Silicon is one of the most important materials in modern semiconductor industry. Meanwhile, owing to its surface having many functional groups, such as Si−H and Si−O, it may provide a good biocompatibility and can be grafted with other functional groups. Si materials including single-crystal Si, porous Si, and Si nanowires have been widely used as the substrates for biochips and biosensors.[16] In our previous work, we have developed a multistep template replication process to produce a highly ordered silicon nanotube (SiNT) array and demonstrated that such a SiNT array displayed excellent field emission properties.[17] To the best of our knowledge, no report on the direct electrochemistry of the redox proteins on the "bare" silicon electrode has been published to date.

In this work, we have mainly investigated the possibility of the SiNT array as an electrode and studied the electrochemical behaviors of redox proteins. The experimental results demonstrate that the hollow structures of SiNT arrays can provide a molecular channel to let the protein easily arrive at the electrode surface, and the surfaces of inner wall of the SiNTs with good biocompatibility and feasibility of chemical modification keep the activity of biomaterial to a great extent.

Experimental Section

Chemicals. All reagents were AR grade unless otherwise stated. High-purity aluminum plate (0.2 mm thick, 99.99+% purity) was obtained from Grinm, China. High-purity gases of hydrogen, argon, ethyne, and silane (purity >99.99%) were purchased from Beijing Huayuan Gases & Chemicals Co. Ltd. Oxalic acid, nickel sulfate, boric acid, and hydrochloric acid were purchased from Beijing Chemical Co. Horse heart cytochrome *c* was obtained from Sigma and used without further purification. All solutions were prepared using deionized water.

Fabrication of SiNT Array Electrodes. Experimental procedures for the fabrication of the SiNT array electrodes are illustrated in Scheme 1. Anodic aluminum oxide (AAO) membranes containing 70 nm-diameter pores were grown by potentiostatic anodization of high-purity aluminum plates in 4% oxalic acid aqueous solution in a water bath. For deposition of the carbon nanotubes (CNTs), the AAO templates were placed in a furnace in an Ar flow of 100 sccm. After the reactor temperature was increased to 650 °C, an ethyne flow of 30 sccm

* Corresponding author. E-mail: dsxu@pku.edu.cn; yhshao@pku.edu.cn.

10.1021/jp0657944 CCC: $37.00
Published on Web 01/25/2007

SCHEME 1: Flow Chart of the Multistep Template Replication Process for Fabrication of Si Nanotube Array Electrodes

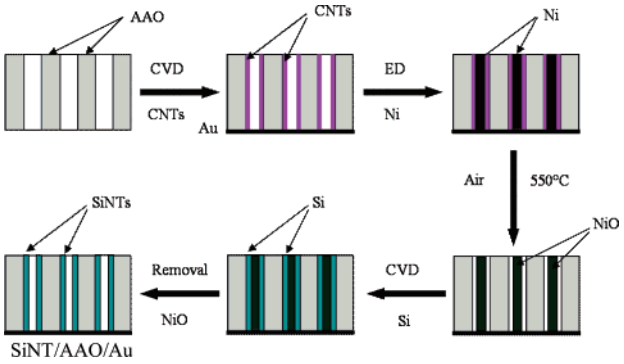

was introduced for 30 min, and then the template membrane was annealed at 650 °C in argon for 10 h prior to its cooling down to room temperature. A gold thin film was coated on one side of the CNT/AAO membrane by vacuum evaporation to make a conductive contact. The electrodeposition of metal was performed potentiostatically in a three-electrode configuration, where a platinum plate, the saturated calomel electrode (SCE), and the CNT/AAO/Au membrane were used as counter, reference, and working electrodes, respectively. Nickel was electrodeposited at a constant voltage of −1.0 V versus SCE in the electrolyte of 0.15 M nickel sulfate and 0.6 M boric acid. After electrodeposition of Ni, the Ni/CNT/AAO membranes were oxidized at 400 °C for 10 h and then heated at 550−600 °C for 2 h in air to gain NiO/AAO annular nanochannel templates. The annular nanochannel templates were placed in an alumina crucible, and the crucible was located at the center of the alumina tube. After evacuating the alumina tube to a pressure below 10^{-2} Torr, Ar gas was input at a flow rate of 100 sccm and kept the pressure at 1.0 kPa. During the growth process of SiNTs, silane gas was introduced into the reaction tube with a flow of 10 sccm for 20 min, and then the temperature was kept at 600 °C for 2 h. After the SiNT/AAO was dissolved in 0.1 M hydrochloric acid for more than 24 h to remove the nickel oxide cores, we obtained the SiNT/Au film with hollow holes as electrode. For comparison, AAO and CNT/AAO were directly evaporated as a gold thin film on one side as electrode.

Electrochemical Cell and Measurements. We chose cytochrome *c*, a structurally and electrochemically well-characterized heme protein,[18] to serve as a simple model in this work. Cyclic voltammetry (CV) was performed with a CHI 660 electrochemical workstation (CH Instruments) in a conventional three-electrode configuration cell with the SiNT array electrode (∼4 mm × 5 mm) as the working electrode, a platinum filament as the auxiliary electrode, and a saturated calomel electrode (SCE) as the reference electrode. The solution concentration was 0.5 mM in a 0.1 M phosphate buffer solution (pH 7.0). The test electrolyte solutions were blown with high-purity nitrogen in order to maintain the solutions anaerobic throughout the electrochemical experiments. All experiments were carried out at room temperature (22 ± 2 °C).

Results and Discussion

Characterization of the Array Electrodes. Scanning electron microscopy (SEM, Quanta200FEG, FEI Co.) was used to characterize the SiNT array. The SEM image of the SiNT array embedded in the AAO template showed that the SiNTs were separated by the alumina wall of the template (Figure 1a). After partial dissolution of the AAO template, these SiNTs tended to

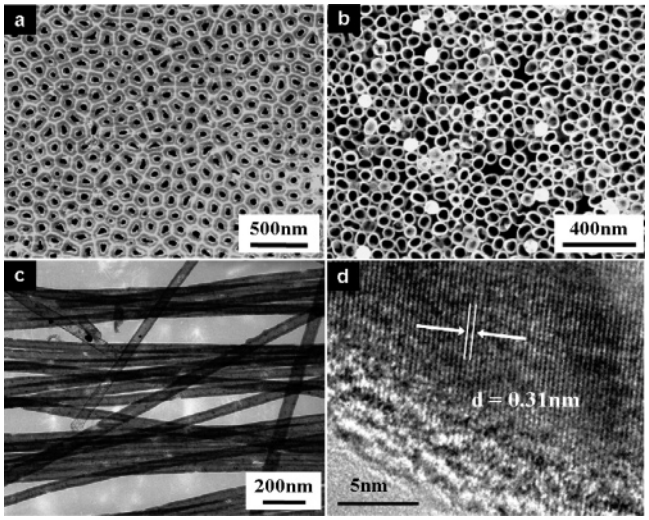

Figure 1. SEM images of the SiNTs (a) after removal of the nickel oxide cores by 1 M HCl and then (b) etched in 0.1% HF for 1 min to partly dissolve the AAO template. (c) Typical TEM and (d) higher-resolution TEM images of the SiNTs.

"stick" to each other, forming a hexagonal pattern (Figure 1b). The average outerpore diameter is about 70 nm with the wall thickness of ∼10 nm (Figure 1c). The lengths of the nanotubes are about 20 μm. Detailed analysis on the lattice images (Figure 1d) gives interplanar spacing of 0.31 nm, closely corresponding to that of Si(111) planes.

Cyclic voltammetry and $K_3Fe(CN)_6$ were also employed to characterize the array electrodes. Figure 2 is the CV responses of the three types of one-dimensional (1D) pore array electrodes in the presence of 2 mM $K_3Fe(CN)_6$ in 1 M $K(NO)_3$ at different sweep rates. Well-defined voltammetric responses are observed at these nanopore electrodes at a potential range of 0.6 to −0.2 V, and the ΔE_p values increase with the sweep rates. The cathodic peak currents were also found to be linearly proportional to the square root of the sweep rates with correlation coefficient of 0.999 (see Figure 2d).

The determination of the active electrode surface can give a direct comparison of the SiNT structure with the flat surface, which is commonly used in the electrochemistry of the nanostructural electrode. We measured the electroactive area of the SiNT electrodes using a mediator whose diffusion coefficient is known. For a 1D pore electrode where the pores are sufficiently deep, it has been demonstrated that the current becomes limited by planar diffusion of redox molecules initially present in the pore and adjacent to the electrode surface.[19] In such a 1D pore system, the Randles−Sevcik expression for the classical planar electrode can still be usable.[20] The value of the electroactive area, *A*, is determined from the slope of a plot of the voltammetric peak current, I_p, versus the square root of sweep rate, $v^{1/2}$:

$$I_p = 2.69 \times 10^5 n^{3/2} A D_0^{1/2} C_0 \nu^{1/2} \quad (1)$$

where *n* is the electron transferred number of the reaction, D_0 is the diffusion coefficient and C_0 is the concentration of the redox species. The slopes of I_p against $\nu^{1/2}$ are 192.4, 388.0, and 619.5 for 2 mM $Fe(CN)_6^{3-}$ at AAO/Au, CNT/Au and SiNT/Au electrodes, respectively. The apparent area of the electrodes is 0.20 cm^2. Here, $n = 1$, $D_0 = 7.6 \times 10^{-6}$ $cm^2 \cdot s^{-1}$, and $C_o = 2 \times 10^{-3}$ M. The apparent electroactive areas of the CNT/Au electrode and the SiNT/Au electrode were calculated to be 0.26 cm^2 and 0.42 cm^2, respectively, which are larger than the

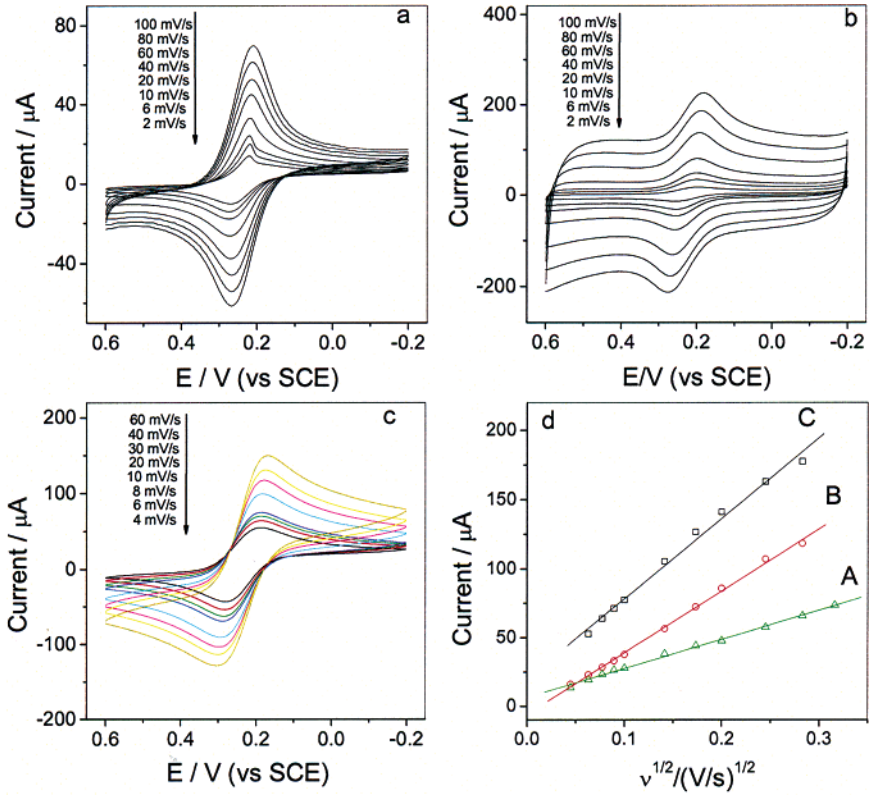

Figure 2. Cyclic voltammograms of three types of nanopore electrode in the presence of 2 mM $K_3Fe(CN)_6$ in 1 M $K(NO)_3$ at different sweep rates: (a) AAO/Au electrode; (b) CNT/Au electrode; (c) SiNT/Au electrode. (d) Plots of the reduction peak current vs the square root of the sweep rate of AAO/Au electrode (A), CNT/Au electrode (B), and SiNT/Au electrode (C).

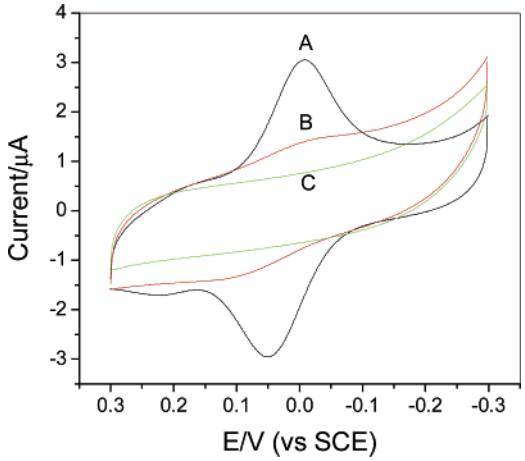

Figure 3. Cyclic voltammograms of the SiNT array electrode (A) and the CNT/Au electrode (B) in the presence of 0.5 mM cytochrome *c* in 0.1 M phosphate buffer solution (pH 7.0). (C) Background CV of the SiNT electrode in 0.1 M phosphate buffer solution (pH 7.0). Sweep rate: 10 mV/s.

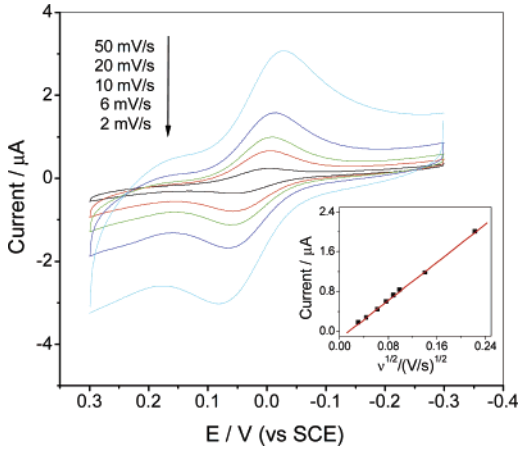

Figure 4. Cyclic voltammograms of the SiNT/Au electrode in the presence of 0.5 mM cytochrome *c* in 0.1 M phosphate buffer solution (pH 7.0) at different sweep rates. Inset: plot of cathodic peak current versus the square root of the sweep rate. Electrode area = 0.20 cm^2.

geometry area of the pores, but smaller than the surface area of the nanotubes in the electrode. In contrast, the electroactive area of AAO/Au electrode without the SiNTs was calculated to be 0.13 cm^2, close to the geometry area of the pores. Therefore, we can conclude that the planar diffusion of the mediator, $Fe(CN)_6^{3-}$, presents in the pore and adjacent to both the Au surface and the surface of the SiNT near to the bottom.

Electrochemical Behaviors of Cytochrome *c* on the SiNT/Au Electrode. The cyclic voltammogram of cytochrome *c* on a bare 70-nm-diameter SiNT/Au electrode with a sweep rate of 10 mV/s is shown in Figure 3A. A well-defined voltammetric response is observed in the potential range of 0.3 to −0.3 V versus SCE. This response was observed immediately upon introducing cytochrome *c* solution into the electrochemical cell. The half-wave potential obtained from the CV is 0.025 V vesus SCE, which is in good agreement with the formal potential of the native cytochrome *c*.[16] The peak separation (ΔE_p) between the anodic and the cathodic peaks is 63 mV, indicating a quasi-reversible process of cytochrome *c* on the SiNT electrode. We also collected voltammograms at the AAO/Au and the CNT/Au electrodes (see Figure 3B for CNT/Au), and there has been no good redox response found. Thus, it is conclusive that the SiNT surface can play a key role in the observation of the good CV response of cytochrome *c*.

Figure 4 shows the voltammetric reponse of cytochrome *c* on the bare SiNT/Au electrode with different sweep rates. In the sweep rate range of 1−50 mV/s, the cathodic peak currents

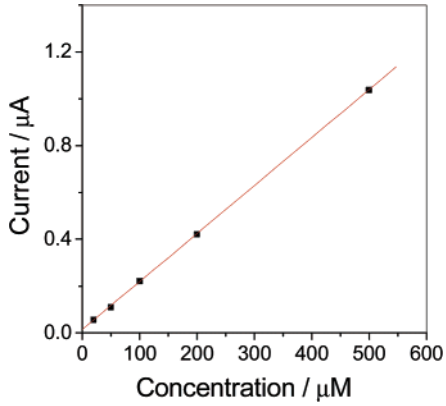

Figure 5. Plot of cathodic peak current as a function of the concentration of cytochrome *c*.

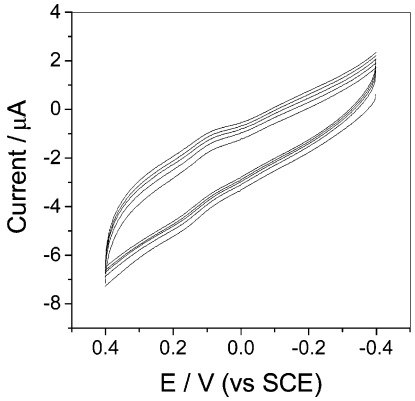

Figure 6. Cyclic voltammograms of the SiNT/Au electrode adsorbed with cytochrome *c*. Sweep rate: 10 mV/s.

were found to be linearly proportional to the square root of the sweep rates with a correlation coefficient of 0.999 (the inset of Figure 4), which corresponds to a planar diffusion controlled response.[17] Figure 5 shows a plot of the cathodic peak current as a linear function of the concentrations of cytochrome *c*. The linear range is from a few μM to 500 μM.

To further confirm that the signals are associated with the diffusion of cytochrome *c*, we carried out a study concerning the voltammetric measurements of the protein adsorbed on the SiNT electrode surface. In this case, the SiNT electrode was dipped into the cytochrome *c* solution and then rinsed and immersed into clean buffer solution. Cyclic voltammograms show that there were faint signal for cytochrome *c* (Figure 6). These results indicate that, in our experiment, the adsorption of cytochrome *c* to the inner surface of SiNT is weak, and free diffusion of cytochrome *c* in the tubes is dominated.

The diffusion coefficient for cytochrome *c*, D_{ox}, was calculated from the slope of the inset plot in Figure 4, the SiNT electroactive area, and the cytochrome *c* concentration, based on eq 1. Here, $n = 1$, $A = 0.29$ cm^2, and $C_o = 5 \times 10^{-4}$ M. The calculation value of D_o is 6.1×10^{-8} cm^2/s. This value is lower than that reported in literatures for cytochrome *c*.[21,22] Furthermore, we can calculate the apparent heterogeneous rate constant, k°_{app}, from the sweep rate dependence (1−50 mV/s) of the peak splitting via the Nicholson method:[23]

$$\psi = \frac{(D_o/D_r)^{\alpha/2}k^o}{[D_o\pi\nu(nF/RT)]^{1/2}} \qquad (2)$$

At 10 mV/s of the sweep rate and 63 mV of the split peak potential (ΔE_p), ψ is 7. The temperature is 293 K, *n* is equal to 1, and the Faraday constant is 96485 J/mol. If $D_o = D_r$, k°_{app} is calculated to be 5.4×10^{-4} cm/s, which is in accordance with the rate constant reported for other bare electrodes.[11,24]

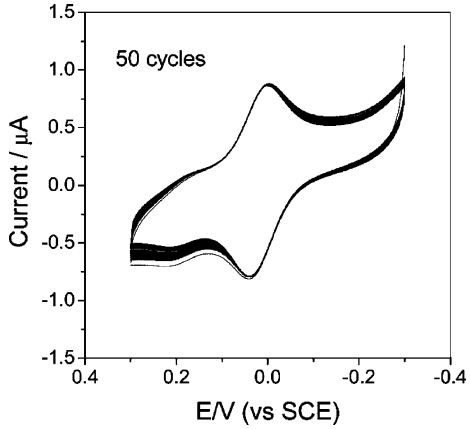

Figure 7. Successive scans of the SiNT array electrode in the presence of 0.5 mM cytochrome *c* in 0.1 M phosphate buffer solution (pH 7.0). Sweep rate: 20 mV/s.

The stability of the electrode is a key factor in the development of novel biosensor devices. Figure 7 displays successive scans of this SiNT array electrode in 0.5 mM cytochrome *c* phosphate buffer solution (pH 7.0) at a sweep rate of 20 mV/s. The response of this SiNT array electrode was found to be stable, and there is no deviation from the initial response after 50 sequential scans. In addition, it was found that this SiNT electrode can give a stable response even after 10 h of CV scans under N_2 atmosphere. Although the Si surface is easily oxidized to SiO_2 in aqueous solution in contact with a gold electrode at positive potentials, the anodic oxidation rate must largely decrease with an increase of the thickness of the SiO_2 layer, because of the increasing resistance of the hole transfer caused by both the insulation of the SiO_2 and the quantum confine effect (QCE) of the SiNT.[25] This assumption was supported by the HRTEM and energy dispersion spectrum observations. In fact, both the crystal structures and the oxygen content of the SiNTs did not show notable changes even after 100 CV scans. In addition, we have done the cyclic voltammetry of the SiNT electrode in the sweep voltage range of −0.9 to approximately +1.0 V versus SCE, indicating that no oxidation peak of Si is found. It is worth to notice that if the SiNT electrode was exposed in air for several days, the SiNT electrode would not provide a good response.

Conclusions

Our experimental results demonstrate that the SiNT arrays are an attractive matrix to accommodate protein and exhibit facile direct electrochemistry of cytochrome *c* without any pretreatment. The facile ET reaction of cytochrome *c* at the bare SiNT electrode can be attributed to the unique properties of SiNTs (e.g., the hollow structures of SiNT arrays which provide a path for cytochrome *c* diffusion, the good electrical conductivity of SiNT,[15] the enhanced surface area arising from the high aspect ratio of the nanotubes, and the good biocompatibility). This methodology described here can be applicable to preparing Si-based third-generation biosensors and protein characterization. Also, it paves a way to study many biological events where biomacromolecules are involved at silicon surfaces. Further studies are required to functionalize the inner- or outerwall of the SiNTs to lead a hydrophilic and negatively charged surface, which would be advantageous to understand the factors that are involved in the heterogeneous ET of cytochrome *c* and other proteins at the SiNT surface.

Acknowledgment. This work is supported by National Natural Foundation of China (Grant Nos. 20433010, 20525309, 20521201, 20235010) and the Major State Basic Research Development Program (Grant No. 2000077503).

References and Notes

(1) Willner, I.; Katz, E. *Angew. Chem., Int. Ed.* **2000**, *39*, 1180−1218.
(2) Wei, J. J.; Liu, H. Y.; Dick, A. R.; Yamamoto, H.; He, Y. F.; Waldeck, D. H. *J. Am. Chem. Soc.* **2002**, *124*, 9591−9599.
(3) Xiao, Y.; Patolsky, F.; Katz, E.; Hainfeld, J. F.; Willner, I. *Science* **2003**, *299*, 1877−1881.
(4) Beissenhirtz, M. K.; Scheller, F. W.; Stocklein, W. F. M.; Kurth, D. G.; Mhwald, H.; Lisdat, F. *Angew. Chem., Int. Ed.* **2004**, *43*, 4357−4360.
(5) Gooding, J. J.; Wibowo, R.; Liu, J. Q.; Yang, W. R.; Losic, D.; Orbons, S.; Mearns, F. J.; Shapter, J. G.; Hibbert, D. B. *J. Am. Chem. Soc.* **2003**, *125*, 9006−9007.
(6) McKenzie, K. J.; Marken, F. *Langmuir* **2003**, *19*, 4327−4331.
(7) Wang, J. X.; Li, M. X.; Shi, Z. J.; Li, N. Q.; Gu, Z. N. *Anal. Chem.* **2002**, *74*, 1993−1997.
(8) Liu, A. H.; Wei, M. D.; Honma, I.; Zhou, H. S. *Anal. Chem.* **2005**, *77*, 8068−8074.
(9) Landrum, H. L.; Salmon, R. T.; Hawkridge, F. M. *J. Am. Chem. Soc.* **1977**, *99*, 3154−3158.
(10) Armstrong, F. A.; Hill, H. A. O.; Oliver, B. N.; Walton, N. J. *J. Am. Chem. Soc.* **1984**, *106*, 921−923.
(11) Haymond, S.; Babcock, G. T.; Swain, G. M. *J. Am. Chem. Soc.* **2002**, *124*, 10634−10635.
(12) Topoglidis, E.; Astuti, Y.; Duriaux, F.; Grätzel, M.; Durrant, J. R. *Langmuir* **2003**, *19*, 6894−6900.
(13) Xu, X.; Tian, B. Z.; Kong, J. L.; Zhang, S.; Liu, B. H.; Zhao, D. Y. *Adv. Mater.* **2003**, *15*, 1932−1936.
(14) Luo, H.; Shi, Z.; Li, N.; Gu, Z.; Zhuang, Q. *Anal. Chem.* **2001**, *73*, 915−920.
(15) (a) Zhao, Q.; Zhan, D.; Ma, H.; Zhang, M.; Zhao, Y.; Jing, P.; Zhu, Z.; Wan, X.; Shao, Y.; Zhuang, Q. *Frontiers in Bioscience* **2005**, *10*, 326−334. (b) Sun, N.; Guan, L.; Shi, Z.; Li, N.; Gu, Z.; Zhu, Z.; Li, M.; Shao, Y. *Anal. Chem.* **2006**, *78*, 6050−6057.
(16) (a) Lin, V. S. Y.; Motesharei, K.; Dancil, K. P. S.; Sailor, M. J.; Gladiri, M. R. *Science* **1997**, *278*, 840−843. (b) Zheng, G. F.; Patolsky, F.; Cui, Y.; Wang, W. U.; Lieber, C. M. *Nat. Biotechnol.* **2005**, *23*, 1294−1301. (c) Wei, F.; Chen, C. L.; Zhai, L.; Zhang, N.; Zhao, X. S. *J. Am. Chem. Soc.* **2005**, *127*, 5306−5307.
(17) Mu, C.; Yu, Y. X.; Liao, W.; Zhao, X. S.; Xu, D. S.; Chen, X. H.; Yu, D. P. *Appl. Phys. Lett.* **2005**, *87*, 113104.
(18) Mathews, F. S. *Prog. Biophys. Mol. Biol.* **1985**, *45*, 1.
(19) Zhang, B.; Zhang, Y. H.; White, H. S. *Anal. Chem.* **2006**, *76*, 477−483.
(20) Bard, A. J.; Faulkner, L. R. *Electrochemical Methods: Fundamentals and Applications*, 2nd ed.; John Wiley & Sons, Inc,: New York, 2001; p 231.
(21) Ehrenberg, A. *Acta Chem. Scand.* **1957**, *11*, 1257−1270.
(22) Theorell, H. *Biochem. Z.* **1936**, *285*, 207−218.
(23) Nicholson, R. S. *Anal. Chem.* **1965**, *37*, 1351−1355.
(24) Sun, S. C.; Reed, D. E.; Cullison, J. K.; Rickard, L. H.; Hawkridge, F. M. *Mikrochim. Acta* **1988**, *3*, 97−104.
(25) Cullis, A. G.; Canham, L. T.; Calcott, P. D. J. *J. Appl. Phys.* **1997**, *82*, 909−965.